PDE Based Enhancement of Color Images in RGB Space

Salim Bettahar, Amin Boudghene Stambouli, Patrick Lambert, Alexandre Benoit

PDE Based Enhancement of Color Images in RGB Space

S. Bettahar, A. B. Stambouli, P. Lambert and A. Benoit

Abstract—**A novel method for color image enhancement is proposed as an extension of scalar diffusion-shock filter coupling model, where noisy and blurred images are denoised and sharpened. The proposed model is based on using single vectors of the gradient magnitude and the second derivatives as a technique to relate different color components of the image. This model can be viewed as a generalization of Bettahar-Stambouli filter to multi-valued images. The proposed algorithm is more efficient than the mentioned filter and some previous works on color image denoising and deblurring without creating false colors.**

Index Terms— **Diffusion, shock filter, color, noise, blur, enhancement.**

I. Introduction

CAPTURING an image with sensors is an important step in many areas. The captured image is used in several applications, which all have their own requests on the quality of the captured image. Acquired images are often degraded with blur, noise or blur and noise simultaneously. The processing to be applied to these images depends on the way of extracting wanted information. So, the frequent problem in low-level computer vision arises from the goal to eliminate noise and uninteresting details from an image, without blurring semantically important structures such as edges [1,2]. Two operations would be done: denoising and sharpening. Since, several deconvolution and denoising techniques have been proposed in the literature: Statistics based filters [3,4,5], wavelets [6,7], Partial Differential Equations (PDE) based algorithms [8,9] and variational methods [10,11]. Particularly, a large number of PDE-based methods have been proposed to tackle the problem of image denoising with a good preservation of edges, and also to explicitly account for intrinsic geometry. In this paper, we are interested in PDE-based methods. Hence, partial differential equations based on diffusion methods [8,12,13,14,15] and shock filter [16,17,18] have recently dominated image processing research, as a very good tool for noise elimination, image enhancement and edge detection [19]. Then many solutions have been proposed in the processing of gray level images by coupling diffusion to shock filter [20,21,22,23,24]. The extension of these methods to multi-valued images can be achieved in two ways. The first one consists in using a marginal approach that enhances each color component of the multi-valued image separately using a scalar method [25]. The second way consists in using a single vector processing, where different components of the image are enhanced by considering correlation between them [15,26,27,28,29,30,31,32].

Manuscript received July 29, 2010.

S. Bettahar and A. B. Stambouli are with the Electronics Department, Electronics and Electrical Engineering Faculty, University of Sciences and Technology of Oran, P.O. Box 1505, El M'naouar, Oran, Algeria (phone: +21341560329; fax: +21341560301; e-mail: salim_bettahar@yahoo.com, aboudghenes@yahoo.com).

P. Lambert and A. Benoit are with the LISTIC, University of Savoie, P.O.Box 80439-74944, Annecy-le-Vieux, (phone: 33450096580; fax: +33450096559; e-mail: patrick.lambert@univ-savoie.fr, alexandre.benoit@univ-savoie.fr).

II. Background

Originated from a well known physical heat transfer process, the PDE- based approaches consist in evolving in time the filtered image *u(t)* under a PDE. When coupling diffusion and shock filter the PDE is a combination of three terms:

$$\frac{\partial u}{\partial t} = C_\eta\, u_{\eta\eta} + C_\xi\, u_{\xi\xi} - C_{sk}\, F\left(u_{\eta\eta}\right)\left|\nabla u\right| \qquad (1)$$

where $u(t=0) = u_0$ is the input image, $|\nabla u|$ is the gradient magnitude, η is the gradient direction, ξ is the direction perpendicular to the gradient, and so $u_{\eta\eta}$ and $u_{\xi\xi}$ represent the diffusion terms in gradient and level set directions respectively. C_η and C_ξ are some flow control coefficients. The first kind of diffusion smoothes edges, while the second one smoothes parallel to the edge on both sides. The last term in (1), which is weighted by C_{sk}, represents the contribution of the shock filter in the enhancement of the image. The function $F(s)$ should satisfy the conditions $F(0)=0$ and $F(s).s \geq 0$. The choice of $F(s) = sign(s)$ gives the classical shock filter [15]. Hence, by considering adaptive weights C_η, C_ξ and C_{sk} as functions of the local contrast, we can favor smoothing process under diffusion terms in homogeneous parts of the image or enhancement operation under shock filter at edge locations.

The first model of coupling diffusion and shock filter has been introduced by Alvarez and Mazorra [20], where the image is diffused only in the direction perpendicular to the gradient eliminating fluctuations and developing shocks with production of false piecewise constant images. This model is given by

$$\frac{\partial u}{\partial t} = C_\xi\, u_{\xi\xi} - sign\left(G_\sigma * u_{\eta\eta}\right)\left|\nabla u\right| \qquad (2)$$

where $*$ denotes the convolution operator, G_σ the Gaussian function with the standard deviation σ and C_ξ is a constant.

However, the balance between diffusion process and shock filter has been more investigated by Kornprobst [21]. It

becomes a binary function of the local contrast in the following scheme:

$$\frac{\partial u}{\partial t}=\alpha_f\left(u-u_0\right)+\alpha_r\left(h_{sk}\,u_{\eta\eta}+u_{\xi\xi}\right)-\alpha_e\left(1-h_{ck}\right)sign\left(G_\sigma * u_{\eta\eta}\right)\left|\nabla u\right| \quad (3)$$

with h_{sk}=1 if $|\nabla u_\sigma| < K$ and 0 otherwise, where K is a contrast threshold. α_f, α_r and α_e are some constants. The parameter K selects edges to be enhanced or smoothed. The first term (u-u_0) is a fidelity term to carry out a stabilization effect of the solution. This reactive term is added as a regularization method in order to oblige the image to be close to the initial one. Kornprobst model is seen also to produce false piecewise constant images.

However, Gilboa developed a complex diffusion shock filter coupling model, that smoothes the image with a weak edges enhancement [22]. The imaginary value of the solution, which is an approximated smoothed second derivative, is used as an edge detector. This filter is given by:

$$\frac{\partial u}{\partial t}=-\frac{2}{\pi}\arctan\left(a\,\mathrm{Im}\left(\frac{u}{\theta}\right)\right)u_\eta+\lambda\,u_{\eta\eta}+\tilde{\lambda}\,u_{\xi\xi} \quad (4)$$

where *Im* denotes the imaginary part of the solution, $\lambda=|\lambda|\,exp(i\theta)$, a and $\tilde{\lambda}$ are real scalars. Gilboa filter is conditioned by the value of θ, which must be smaller than 5° in order to end to the edge detector $\mathrm{Im}\left(\frac{u}{\theta}\right)$ [21].

In the other hand, Fu developed a region-based shock-diffusion scheme [23], where directional diffusion and shock terms are factored by adaptive weights. It is based on the following equation:

$$\frac{\partial u}{\partial t}=C_\eta\,u_{\eta\eta}+C_\xi\,u_{\xi\xi}-w\left(u_\eta\right)sign\left(G_\sigma * u_{\eta\eta}\right)\left|\nabla u\right| \quad (5)$$

C_ξ is used to prevent excess smoothness to smaller details under gradient direction smoothing. C_η, C_ξ and $w(u_\eta)$ are computed by:

	C_η	C_ξ	$w(u_\eta)$
$\|\nabla u_\sigma\| > T_1$	0	$1/(1+l_1\,u_{\xi\xi}^2)$	1
$T_2 < \|\nabla u_\sigma\| \le T_1$	0	$1/(1+l_1\,u_{\xi\xi}^2)$	$\|\mathrm{th}(l_2\,u_{\eta\eta})\|$
else	1	1	0

The thresholds T_1 and T_2 are used to select which edge to be enhanced or smoothed. l_1 and l_2 are constants.

This scheme uses an hyperbolic tangent membership function th($l_2\,u_{\eta\eta}$) to guarantee a natural smooth transition, by controlling softly changes of grey levels of the image. However, Fu filter creates a strong shock between regions of the image, which is due to the oscillations at big edges that make this scheme instable.

In a more recent work, Bettahar and Stambouli proposed a new reliable and stable scheme, which is a kind of coupling diffusion to shock filter with reactive term [24]. This model is based on the following set:

$$\begin{cases}\dfrac{\partial u}{\partial t}=|\nabla u|\,div\left(g\left(|\nabla u_\sigma|\right)\dfrac{\nabla u}{|\nabla u|}\right)-\alpha\left|\nabla\left(f\left(|\nabla u_\sigma|\right)\right)\right|^2(u-v)\\ \dfrac{\partial v}{\partial t}=\beta\left(1-\left|\nabla\left(f\left(|\nabla u_\sigma|\right)\right)\right|^2\right)u_{\eta\eta}-sign\left(G_\sigma * u_{\eta\eta}\right)|\nabla u|\end{cases} \quad (6)$$

where u_σ is the smoothed image using the Gaussian kernel, $v(t)$ is the just previous evolution of $u(t)$. In discrete time, $v(t)$ is the last value of $u(t)$ and $u(0)=u_0$. $g(|\nabla u_\sigma|)$ and $f(|\nabla u_\sigma|)$ are decreasing functions having the same form with free parameters respectively k_d (for g) and k_c (for f), so:

$$g(s)=\frac{1}{1+\dfrac{s^2}{k_d^2}} \quad (7)$$

The first function $g(|\nabla u_\sigma|)$ is used to assure an anisotropic behavior, and to select "small edges" to be smoothed according to the parameter k_d. However, $f(|\nabla u_\sigma|)$ is introduced to select which "big edges" have to be improved according to k_c. The parameters α and β are positive balance constants. All mentioned models have been developed for enhancement of grey levels images. The natural way to apply them on multi-valued images is to process each color component independently of the others in a marginal way. Such a way is well known to produce false colors as it can be observed on fig. 1, whatever the used filter (near parrot eye for instance).

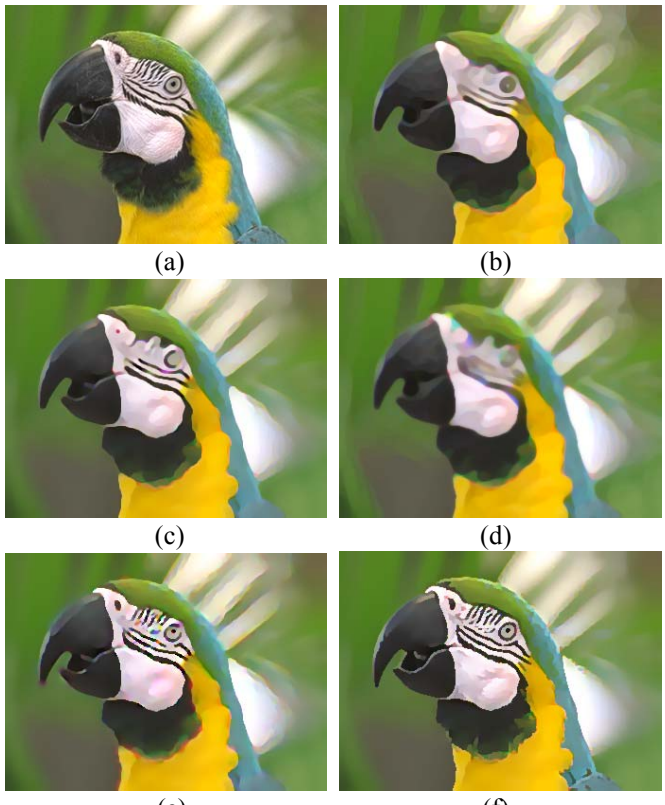

(a) (b) (c) (d) (e) (f)

Fig. 1. Enhancement of Parrot image: (a) Original image; (b) Alvarez-Mazorra filter; (c) Kornprobst filter; (d) Gilboa filter; (e) Fu filter; (f); Bettahar-Stambouli filter.

III. Color Images

Only a very few works tackle the shock diffusion coupling using an approach specifically dedicated to color images [30].

A. Tschumperlé-Deriche model

To avoid the effect of the apparition of false colors, the processing applied to the image must be driven in a common and coherent manner for all image components. This type of approach is denoted as "vector processing", in opposition to the marginal processing which is a multi-scalar processing. Thus, in order to describe vector-valued image variations and structures, Di Zenzo [26] and Lee [27] have proposed to use the local variation of a vector gradient norm $|\nabla u|$ that detects edges and corners when its value becomes high. It can be computed using the eigen-values λ_+ and λ_- ($\lambda_+ > \lambda_-$) of the symmetric and semi-positive matrix G:

$$G=\begin{pmatrix} g_{11} & g_{12} \\ g_{21} & g_{22} \end{pmatrix}=\begin{pmatrix} u_{1x}^2+u_{2x}^2+u_{3x}^2 & u_{1x}u_{1y}+u_{2x}u_{2y}+u_{3x}u_{3y} \\ u_{1x}u_{1y}+u_{2x}u_{2y}+u_{3x}u_{3y} & u_{1y}^2+u_{2y}^2+u_{3y}^2 \end{pmatrix} \quad (8)$$

where u_{pl} (p=1,2,3 and $l = x,y$) represents the derivative in direction l of the red, green and blue components of the color image, and:

$$\lambda_{\pm}=\frac{g_{11}+g_{22}\pm\sqrt{(g_{11}-g_{22})^2-4g_{12}^2}}{2} \quad (9)$$

Three different choices of vector gradient norms can be considered. $\sqrt{\lambda_+}$, which is the value corresponding to the maximum variations. $\sqrt{\lambda_+-\lambda_-}$ that fails to detect saddle points discontinuities. $\sqrt{\lambda_++\lambda_-}$ that detects perfectly edges and corners. Remark that for the eigen-values λ_+ and λ_- correspond the eigen-vectors respectively θ_+ and θ_-, that form an orthogonal base. This new base can be used for geometrical description of the multi-valued image [27].

Hence, by using multi-valued geometrical description of [26,27], Tschumperlé and Deriche proposed a new form of diffusion shock filter coupling especially for enhancement of color images [30]. This model takes into account the correlation between all color components by using the new directions θ_+ and θ_- (η and ξ for the scalar case), where diffusion and shock terms are computed using common directions for all channels. So, in order to evolve all components in same directions, Tschumperlé and Deriche enhanced the image by:

$$\frac{\partial u_p}{\partial t}=a_a\left(u_p-u_{p0}\right)+C_{\theta_-}\left(u_{p\theta_-\theta_-}\right)+C_{\theta_+}\left(u_{p\theta_+\theta_+}\right)-C_{sk}\,sign\left(u_{p\theta_+\theta_+}\right)\left|u_{p\theta_+}\right| \quad (10)$$

where p=1,2,3 for red, green and blue color. a_a is a constant, C_{θ_-} and C_{θ_+} are decreasing functions of the common gradient magnitude $|\nabla u|$, which is computed by the norm:

$$|\nabla u|=\sqrt{\lambda_++\lambda_-}=\sqrt{\sum_{l\in\{x,y\}}\sum_{p=1}^{3}u_{pl}^2} \quad (11)$$

and

$$C_{\theta_-}(s)=\frac{1}{\sqrt{1+s^2}} \quad (12)$$

$$C_{\theta_+}(s)=\frac{1}{1+s^2} \quad (13)$$

C_{sk} is a weight that adapts the intensity of the shock filter process in order to enhance edges, while keeping homogeneous regions unchanged. C_{sk} is obtained using an increasing function of the common gradient magnitude $|\nabla u|$. The relative importance of C_{sk} is empirically tuned.

So, once the new base $\theta_{\pm}=\begin{pmatrix}\theta_{1\pm}\\ \theta_{2\pm}\end{pmatrix}$ is established, it will be easy to compute different partial derivatives as:

$$u_{p\theta_+}=\theta_{1+}u_{px}+\theta_{2+}u_{py} \quad (14)$$

$$u_{p\theta_\pm\theta_\pm}=\theta_{1\pm}^2u_{pxx}+2\theta_{1\pm}\theta_{2\pm}u_{pxy}+\theta_{2\pm}^2u_{pyy} \quad (15)$$

This model gives satisfactory results, in that it removes noise and enhances multi-valuated images. However, despite the use of a vector approach, the shock filter still generates some false colors, as it can be seen in fig. 2. Furthermore, there are some instabilities along edges.

Fig. 2. Enhancement of Parrot image image: (a) Blurry and noised; (b) Tschumperlé-Deriche filter.

B. Proposed method

The proposed method is based on the model (6) as an extension to multi-valued images, where each color component u_p of the enhanced image u is considered by taking into account the correlation between the three components. This model is given by:

$$\begin{cases}\dfrac{\partial u_p}{\partial t}=|\nabla u|\,div\left(g\left(|\nabla u_\sigma|\right)\dfrac{\nabla u_p}{|\nabla u|}\right)-\alpha\dfrac{\left|\nabla\left(f\left(|\nabla u_\sigma|\right)\right)\right|^2}{1+\beta\left|\nabla\left(f\left(|\nabla u_\sigma|\right)\right)\right|^2u_{\xi\xi}^2}\left(u_p-v_p\right)\\ \dfrac{\partial v_p}{\partial t}=-sign\left(G_\sigma*u_{\eta\eta}\right)|\nabla u_p|\end{cases} \quad (16)$$

where $v_p(t)$ is the last evolution of $u_p(t)$ and $v_p(0)=u_{p0}$. In discrete time, $v_p(t)$ is the last value of $u_p(t)$. So first, we compute the second equation that gives the value of v_p, which will be injected in the first equation being, later, noted u_p (This point can be well understood by using the discrete form in equations 33 and 34). The functions $g(|\nabla u_\sigma|)$ and $f(|\nabla u_\sigma|)$

are defined by (7) with control parameters respectively k_d and k_c. α and β are constants.

Starting from grey level Bettahar-Stambouli solution, equations (16) has been obtained using an empirical approach but always conserving the constraint that gradient information has to be obtained in a vector way. In these equations, each component is processed separately, like in a marginal approach. However, the processing of each component takes into account the correlation between the different components of the multi-valued image by using the same gradient magnitudes (∇u and ∇u_σ) and the same derivatives ($u_{\xi\xi}$ and $u_{\eta\eta}$) obtained in vector way. This is the key point of the proposed approach which will avoid the generation of false colors, as it will be seen in the following behavior of the proposed model.

The gradient magnitudes are computed by using the equation (11) like in Tschumperlé-Deriche model, while we estimate the second derivatives by:

$$u_{\eta\eta} = \sum_{p=1}^{3} u_{p\,\eta\eta} \tag{17}$$

$$u_{\xi\xi} = \sum_{p=1}^{3} u_{p\,\xi\xi} \tag{18}$$

The sum of the derivatives is a simple but efficient solution to relate different color components. On can use the higher order derivatives given by equation (15), with the risk of creation of false colors while coupling diffusion process to shock filter as in Tschumperlé-Deriche model.

The first equation in the proposed filter behaves as a nonlinear reaction-curvature diffusion process like in (6). In this equation, the first term $|\nabla u|\, div\left(g\left(|\nabla u_\sigma|\right)\frac{\nabla u_p}{|\nabla u|}\right)$ is used to assure a selective smoothing that reduces noise in homogeneous parts of the image without introducing new structures like false colors. The second term $\alpha\frac{\left|\nabla\left(f\left(|\nabla u_\sigma|\right)\right)\right|^2}{1+\beta\left|\nabla\left(f\left(|\nabla u_\sigma|\right)\right)\right|^2 u_{\xi\xi}^2}$ acts as a balance between smoothing of diffusion process and enhancement of shock filter. It is weak in smooth parts and strong at edge locations. Hence, in homogeneous regions, $|f(|\nabla u_\sigma|)| \to 1$, so $|\nabla f(|\nabla u_\sigma|)| \to 0$ and $u_{\xi\xi} \to 0$, while at edge locations $|f(|\nabla u_\sigma|)| \to 0$, so $|\nabla f(|\nabla u_\sigma|)| \to 1$. So, by choosing adequate values of α and β, the weight $\alpha\frac{\left|\nabla\left(f\left(|\nabla u_\sigma|\right)\right)\right|^2}{1+\beta\left|\nabla\left(f\left(|\nabla u_\sigma|\right)\right)\right|^2 u_{\xi\xi}^2}$ will be high at edge locations and low in smooth parts. Thus in the first case the process will operate as a diffusion-shock filter reaction that enhances edges, and in the second case the filter will behave as a linear diffusion that smoothes noise. The second equation in (16) is a simple shock filter and its result $v_p(t)$ is injected in the first equation as a reactive term. It can be noted again that this filter is not designed in a marginal way because of the use of the vector derivative $u_{\xi\xi}$, which is a combination of the values of $u_{p\,\xi\xi}$ (see equation 18).

To well understand the proposed filter behavior, it is necessary to give more details about the reasons which have decided the form of the equation (16). First the choice of the balance diffusion-shock filter, with the form $\alpha\frac{\left|\nabla\left(f\left(|\nabla u_\sigma|\right)\right)\right|^2}{1+\beta\left|\nabla\left(f\left(|\nabla u_\sigma|\right)\right)\right|^2 u_{\xi\xi}^2}$, has a critical impact on the behavior of the proposed model at non creation of false colors. This choice has been done by considering some practical observations on different cases in order to take the best choice of this balance as following. Consequently, by using the marginal method, we have computed the balance $\alpha|\nabla f(|\nabla u_{p\sigma}|)|^2$ of the model (6) with processing each image component separately. We can observe in this case some false colors at edge locations as an expected result (fig. 3-b).

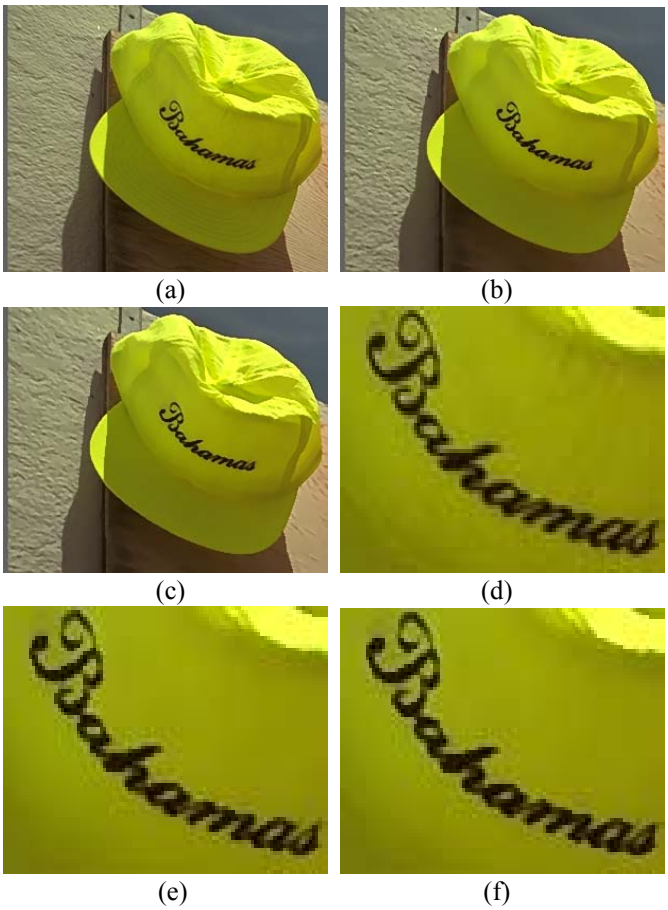

(a) (b) (c) (d) (e) (f)

Fig. 3. Enhancement of Cap image; (a) Original image; (b) Using the marginal balance $\alpha|\nabla f(|\nabla u_{p\sigma}|)|^2$; (c) Using the balance $\alpha\frac{\left|\nabla\left(f\left(|\nabla u_\sigma|\right)\right)\right|^2}{1+\beta\left|\nabla\left(f\left(|\nabla u_\sigma|\right)\right)\right|^2}$;(d) Enlargement of situation (a); (e) Enlargement of situation (b); (f) Enlargement of situation (c).

However, by applying the balance $\alpha\frac{\left|\nabla\left(f\left(\left|\nabla u_\sigma\right|\right)\right)\right|^2}{1+\beta\left|\nabla\left(f\left(\left|\nabla u_\sigma\right|\right)\right)\right|^2}$ that uses the vector method, it can be noticed in fig. 3-c that the image has been enhanced without creating any false colors. This can be well remarked on the enlargement of "Bahamas" text, where some red and green colors have been created in the first case (fig. 3-e). Second, by introducing the term $u_{\xi\xi}$, we can make the model more robust at creation of false colors in the case of noisy images. We consider now a single gradient vector ∇u for all color image components. So we compare performances of the proposed model, firstly by using the balance $\alpha|\nabla f(|\nabla u_\sigma|)|^2$ (β =0), and secondly by introducing in the dominator of the proposed balance the term $1+\beta|\nabla f(|\nabla u_\sigma|)|^2 u_{\xi\xi}$. As depicted in fig. 4, noise has been removed successfully in both cases, but in the first one (fig. 4-e) false colors at edges locations have been created.

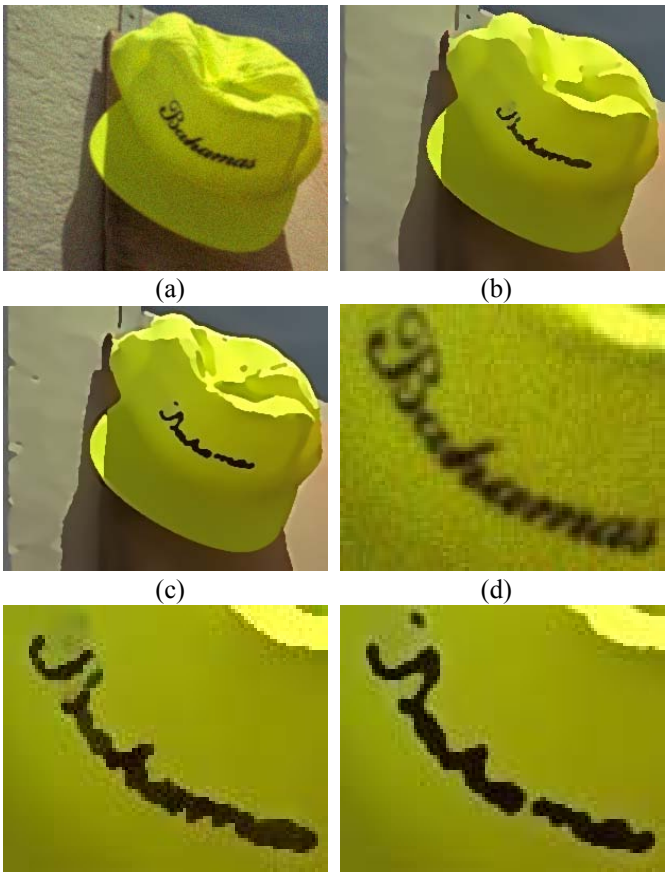

Fig. 4. Enhancement of Cap image; (a) Noisy image; (b) Using the balance $\alpha\nabla|f(|\nabla u_\sigma|)|^2$ (β = 0 in eq. (16)); (c) Using the balance $\alpha\frac{\left|\nabla\left(f\left(\left|\nabla u_\sigma\right|\right)\right)\right|^2}{1+\beta\left|\nabla\left(f\left(\left|\nabla u_\sigma\right|\right)\right)\right|^2 u_{\xi\xi}^2}$; (d) Enlargement of situation (a); (e) Enlargement of situation (b); (f) Enlargement of situation (c).

Structures in the results of models 6 and 16 being close, it is interesting to note that the proposed method produces so similar results than Bettahar-Stamboui filter when it is applied on grey level images (fig. 5).

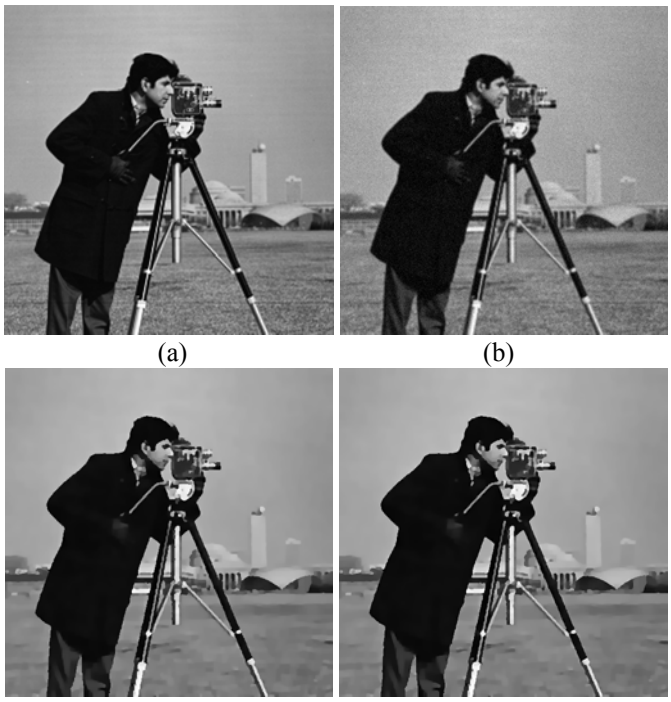

Fig. 5. Enhancement of Cameraman image: (a) Original image; (b) Blurry and noised image; (c) Bettahar-Stambouli filter; (d) Proposed filter.

The choice of the parameters has a critical impact on the behavior of the proposed filter. So, with reference to the contrast of the image, the value of k_d is chosen to be a threshold of "small edges" to be smoothed under the diffusion process and k_c "big edges" to be improved according to the shock filter. One can use the same values for the threshold dedicated to "big" and "small" edges in both Bettahar 's filters. In our experiences, we saw that in this case the filters converge to the solution with a considerable number of iterations without good detail preservations comparing to the case of k_c=k_d.

The constants α and β contribute in the balance between the diffusion process and the shock filter. If we want to attenuate the effect of the shock filter, we have to take small α and large value of β.

Recently, an interesting method called block-matching and 3D filtering (BM3D) has been developed by Dabov [5] and improved by Hou [33]. This method is based on Wiener filtering that requires *a priori* knowledge about the noise. In the case of PDE coupling, no knowledge about the blur or the noise is needed. As depicted in fig. 6, our model gives almost similar results in smoother regions with an effective edge

sharpening compared to the BM3D based method. This latter has the drawback of not eliminating the blur.

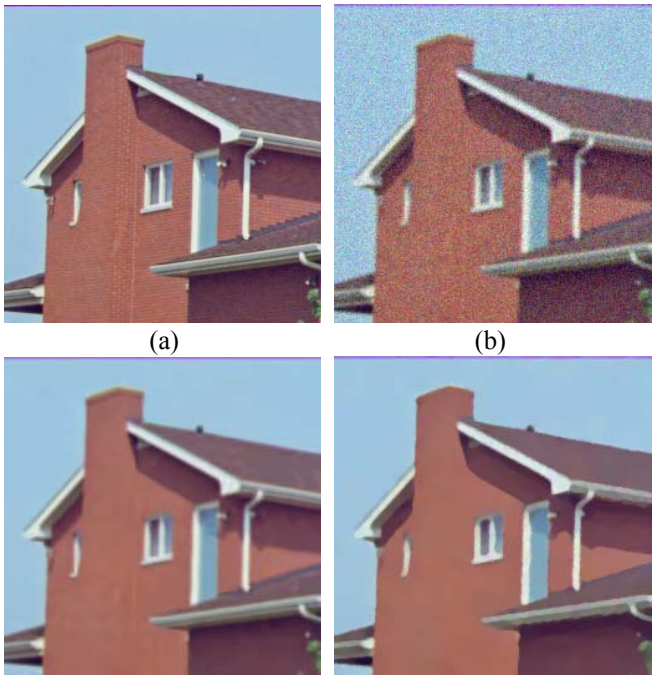

(a) (b) (c) (d)

Fig. 6. Enhancement of House image: (a) Original image; (b) Blurry and noised image; (c) BM3D filter (d) Proposed filter;.

IV. Experimental Results

We evaluate performances of our model by comparing it to marginal channel by channel methods of Alvarez-Mazorra, Kornprobst, Gilboa, Fu, Bettahar-Stambouli and the vector regularization of Tschumperlé-Deriche only. These are developed especially to enhance degraded images in presence of blur and additive noise simultaneously. We are not dealing with the evaluation of other types of methods, as our focus is on diffusion-shock filter coupling.

A. Direct observation

For this comparison, we choose the parameters that give better results for each filter, except for the number of iterations which must be the same for objective comparison. The number of iterations is chosen in function of the visual quality of the result. For each test image, we opt for the same number of iterations, and for the step time τ we prefer a small value in order to converge to the solution with more precision about the values of the objective criterions while getting more details in the visual aspect of the restored images. So, we can converge to the solution with small numbers of iterations in reference to the number that we use in this paper, excepted to Tschumperlé-Deriche filter that employs an adaptive step time τ. All models are applied to blurry and noised images. In the production of artificially blurry images, we use the Gaussian convolution of original test images (σ=1). Noised images are produced by adding random Gaussian noise to blurred images (σ=18). The first criterion used is the color Pick Signal to Noise Ration (PSNR):

$$PSNR=10\log_{10}\left(\frac{255*255}{\sum_{p=1}^{3}\sum_{i=1}^{M}\sum_{j=1}^{N}\left(I_p(i,j,p)-u_p(i,j,p)\right)^2}\right) \quad (19)$$

Where I_p is the p component of the color image reference $I(M\text{x}N\text{x}3)$ and u_p is the p component of the restored image $u(M\text{x}N\text{x}3)$.

For more objective comparison of overall image qualities, we also use the Mean Image Quality Assessment Index MSSIM [34], which is given by the following expression as for one component p :

$$MSSIM_p=\frac{\left(2\mu_{p_0}\mu_p+C_1\right)\left(2\sigma_{0p}+C_2\right)}{\left(\mu_{p_0}^2+\mu_p^2+C_1\right)\left(\sigma_0^2+\sigma_p^2+C_2\right)} \quad (20)$$

where σ_0 and σ_p are the standard deviations of the images I_p and u_p respectively. μ_p is the mean value of the image u_p ,

$$\sigma_{0p}=\frac{1}{MN}\sum_{i=1}^{M}\sum_{j=1}^{N}\left(I_p(i,j)-\mu_{p_0}\right)\left(u_p(i,j)-\mu_p\right) \quad (21)$$

and where C_1 and C_2 are small constants that provide stability when the denominator approaches zero. The MSSIM for the color image is the mean value of the MSSIM obtained for each component.

Fig. 7 shows Face image blurred and noised with PSNR=18.10 dB. We use for Alvarez-Mazorra filter σ=1, C=2 and the time step discretization τ=0.01; Kornprobst filter σ=1, K=3, α_f=0, α_r= 1, α_e=1 and τ=0.01; Gilboa filter $\tilde{\lambda}$ =1.5, $|\lambda|$=0.6, a=6, $\theta=\pi/1000$ and τ=0.01; Fu filter σ=1, T_1=35, T_2=4, l_1=0.0008 l_2=200 and τ=0.01; Bettahar-Stambouli filter σ=1, k_d=4, k_c=30, α=800, β=0.05 and τ=0.01; Tschumperlé-Deriche filter α_a=0 and adaptive τ=2; Proposed filter σ=1, k_d=5, k_c=28, α=800, β=1 and τ=0.01 with 1500 iterations for all mentioned filters. We easily notice that our model has efficiently removed noise in smoother regions with edges sharpening referring to Alvarez-Mazorra, Kornprobst, Gilboa, Bettahar-Stambouli and Tschumperlé-Deriche filters. Only the last two models have successfully smoothed noise in homogeneous parts of the images. The other models have produced false piecewise constant images with residual noise, where artificial blobs have been created. Furthermore, we notice here how Alvarez-Mazorra, Kornprobst, Gilboa and Bettahar-Stambouli filters have introduced false colors as it appears on the different parts of the enhanced image, as on the nose, sun glass edges and cap borders at blue and white junction. Only Tschumperlé-Deriche model presents some satisfactory results, with, however, a fine production of false colors at localized edges. On the contrary, in the proposed filter, edges can well be distinguished without any false colors. This is more obvious in fig. 8, on the enlargement of a part of the image, where we can see that our algorithm doesn't create false colors referring to other models with an effective

selective smoothing of the sun glass according to the other parts of the image.

In fig. 9, we present the PSNR evolution versus the number of iterations for the different approaches which have been compared. It can be noted that, for a same number of iterations, the PSNR of our solution is always bigger than the PSNR of other models. This can be deep-rooted by the MSSIM representation (fig. 10), that confirms the best visual quality of our solution.

Fig. 7. Enhancement of Face image: Blurry and noised image; (b) Alvarez-Mazorra filter; (c) Kornprobst filter; (d) Gilboa filter; (e) Fu filter; (f) Bettahar-Stambouli filter; (g) Tschumperlé-Deriche filter; (f) Proposed filter.

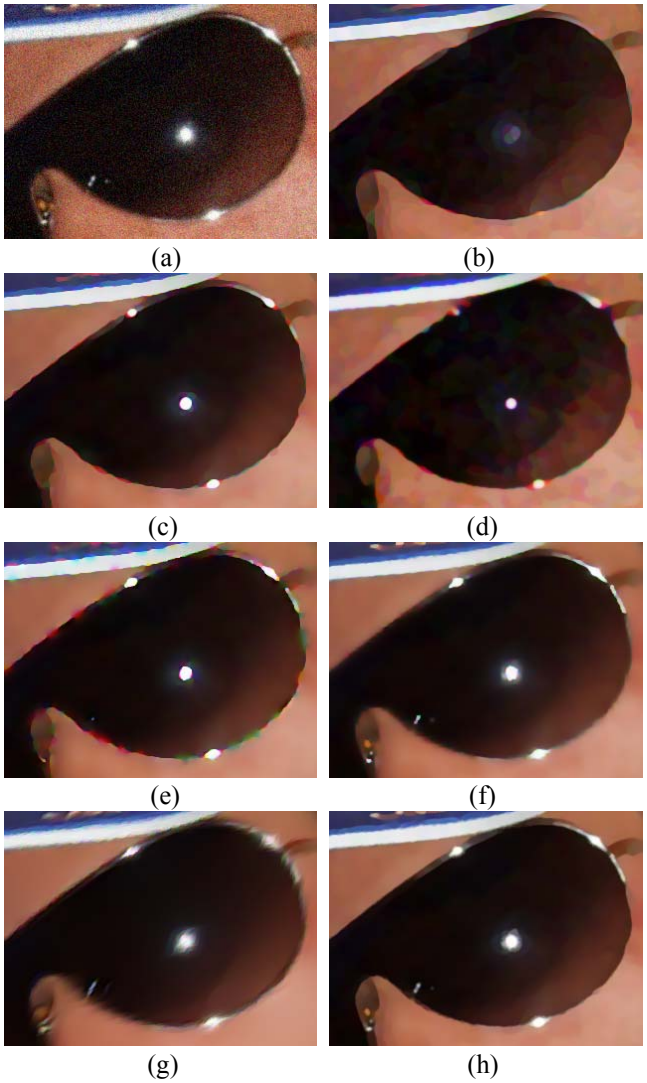

Fig. 8. Enlargement of a part of Face image: (a) Blurry and noised image; (b) Alvarez-Mazorra filter; (c) Kornprobst filter; (d) Gilboa filter; (e) Fu filter; (f) Bettahar-Stambouli filter; (g) Tschumperlé-Deriche filter; (h) Proposed filter.

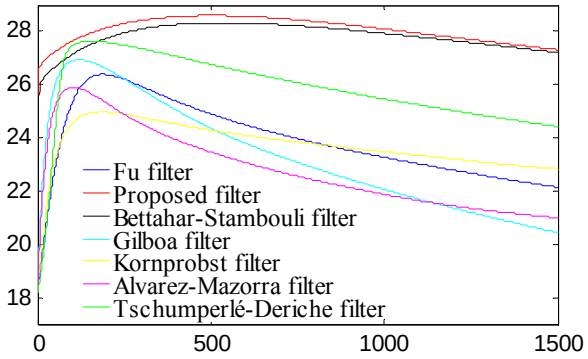

Fig.9. PSNR representation of Face image as a function of the number of iterations.

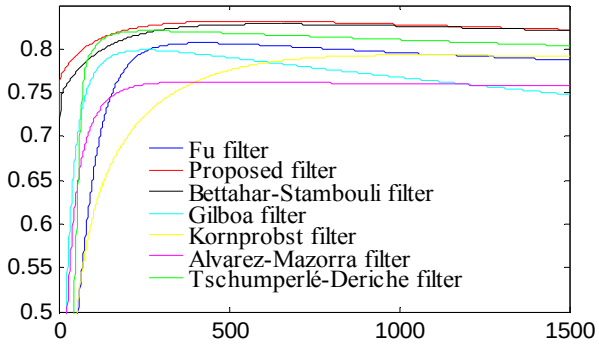

Fig. 10. MSSIM representation of Face image as a function of the number of iterations.

The second experiment has been performed on blurred and noised Window-Flowers image with strong noise PSNR=17.67 dB (fig. 11). We use for Alvarez-Mazorra filter σ=1, C=2 and τ=0.05; Kornprobst filter σ=1, K=2, α_f=0, α_r=1, α_e=1 and τ=0.05; Gilboa filter $\tilde{\lambda}$=1, $|\lambda|$=0.5, a=6, θ=π/1000 and τ=0.05; Fu filter σ=1, T_1=25, T_2=2, l_1=0.0008 l_2=200 and τ=0.05; Bettahar-Stambouli filter σ=1, k_d=2, k_c=30, α=800, β=0.05 and τ=0.05; Tschumperlé-Deriche filter α_a=0 and adaptive τ=2 ; Proposed filter σ=1, k_d=3, k_c=110, α=800, β=1 and τ=0.05 with 500 iterations for all filters. We can see here again how our method has removed noise in homogeneous parts of the image without creating false colors referring to other models. In our case, the window, flowers and sheets are well denoised and sharpened as observed in fig. 12, where the window and the pink flower are successfully enhanced. Only Tschumperlé-Deriche model gives satisfactory results, but we can see a subsistence of a kind of false colors on the horizontal lines of the window and on a part of the pink flower. In the case of Alvarez-Mazorra, Kornprobst, Gilboa and Bettahar-Stambouli filters, a residual noise subsists with false colors at edge locations.

In fig. 13, we remark that our PSNR is always bigger than the PSNR of other models with a better MSSIM (fig. 14). Looking at the PSNR and MSSIM evolutions, it is also interesting to compare the proposed approach to Bettahar-Stambouli marginal approach. As these methods principles are close, this specific comparison is a measure of the difference between the marginal approach and the vector approach. It can be concluded that using a vector approach always provides a gain, even though this gain is sometimes small.

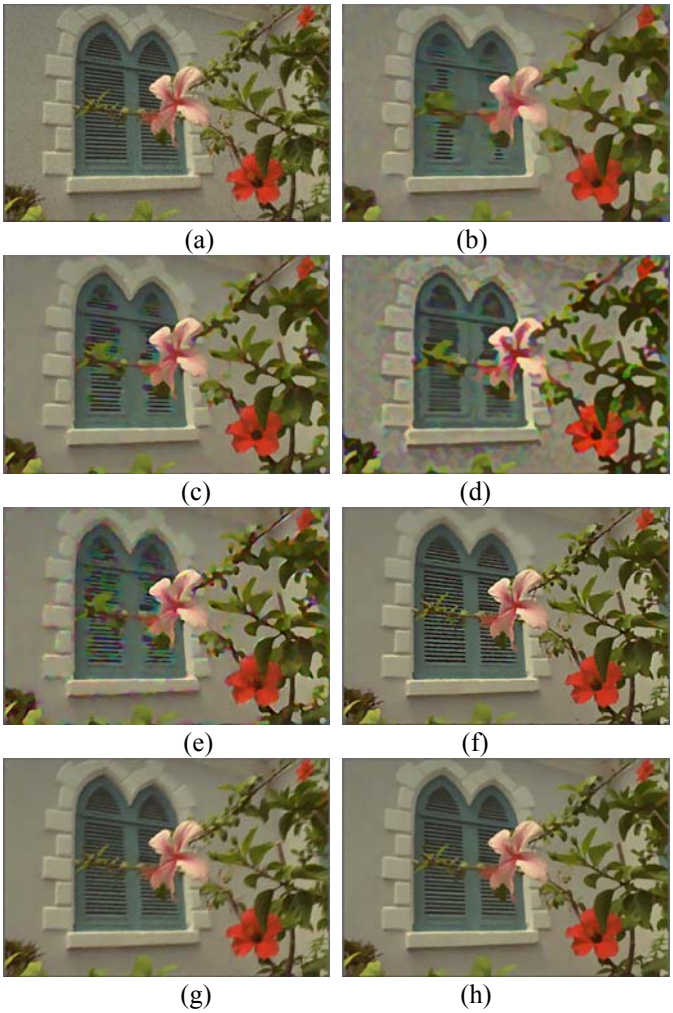

Fig. 11. Enhancement of Flowers-Window image: Blurry and noised image; (b) Alvarez-Mazorra filter; (c) Kornprobst filter; (d) Gilboa filter ; (e) Fu filter; (f) Bettahar-Stambouli filter; (g) Tschumperlé-Deriche filter; (f) Proposed filter.

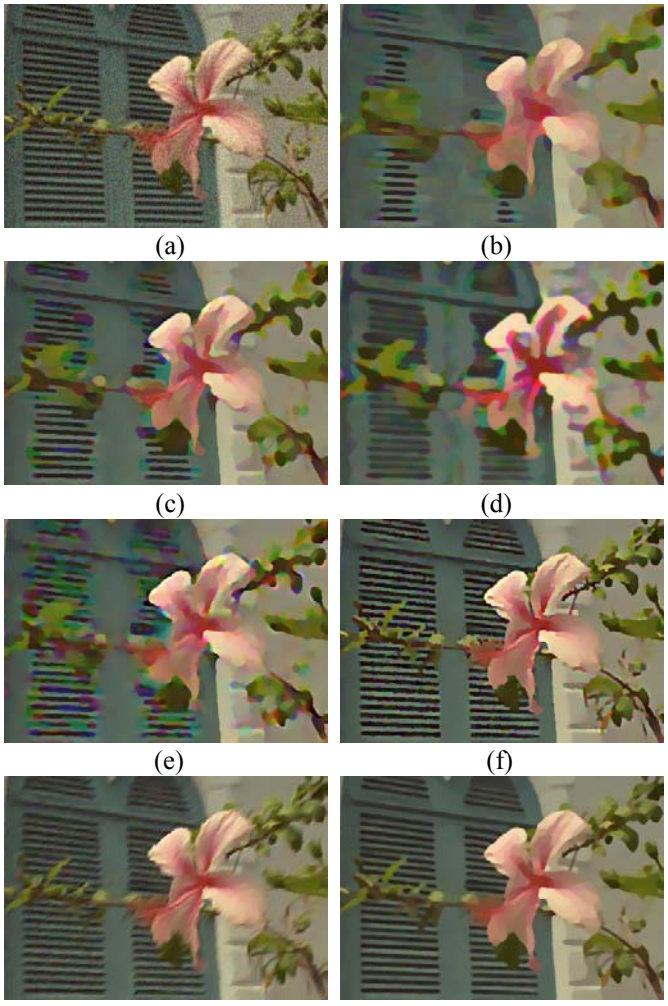

Fig. 12. Enlargement of a part of Flowers-Window image: (a) Blurry and noised image; (b) Alvarez-Mazorra filter; (c) Kornprobst filter; (d) Gilboa filter ; (e) Fu filter; (f) Bettahar-Stambouli filter; (g) Tschumperlé-Deriche filter; (h) Proposed filter.

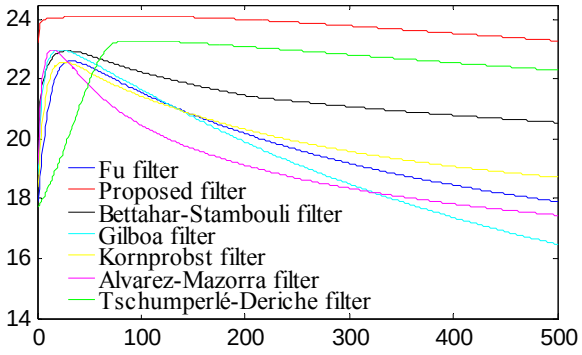

Fig. 13. PSNR representation of Flowers-Window image as a function of the number of iterations.

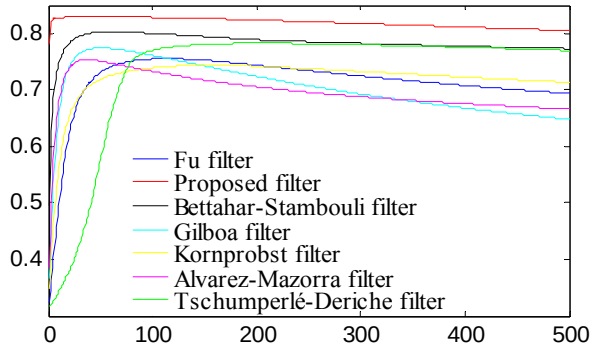

Fig. 14. MSSIM representation of Flowers-Window image as a function of the number of iterations.

B. Indirect observation

Filtering is generally a pre-processing before segmentation. So, an indirect way to compare different filtering approaches is to compare the segmentation obtained after filtering.

a – Edge detection

The first comparison is performed after edge detection. The image which is used is the Flowers-Window image seen in fig. 11. Edges are obtained using the marginal Canny edge detector. We can obviously observe how edges in our solution are well detected and closed referring to other methods that present thin contours due to the presence of false colors at edge locations (fig. 15). These observations show how performances of our model are improved in presence of a strong noise.

b – Region segmentation

The second comparison is performed after region segmentation. The segmentation which is used is a classical region growing technique: blob-coloring using a 4 neighborhood [35]. This technique is a quick and simple one which is known to give over-segmentation, providing a lot of small regions in noisy situation. In our case, this drawback will be used to extract a measure of performance. Nevertheless, to limit over-segmentation, the region growing is realized iteratively, the aggregation threshold being incremented at each iteration. Fig. 16 shows the results of the segmentation on Face image. All the different segmentations have been realized using the same parameter values (initial threshold = 3, threshold increment = 2, iteration number = 30).

On this figure, it can be seen that the simplest segmentation is the one obtained with the proposed method, despite the largest number of regions. Tschumperlé-Deriche and our method excepted, all the segmentations contain false regions due to false colors. Alvarez-Mazorra and Gilboa give an over-segmentation in the background, on the face and on the glasses. Kornprobst, Fu and Bettahar-Stambouli provide some quite good segmentations, but with false color regions. With Tschumperlé-Deriche filter, there are thin regions along some edges, like the borders of the glasses.

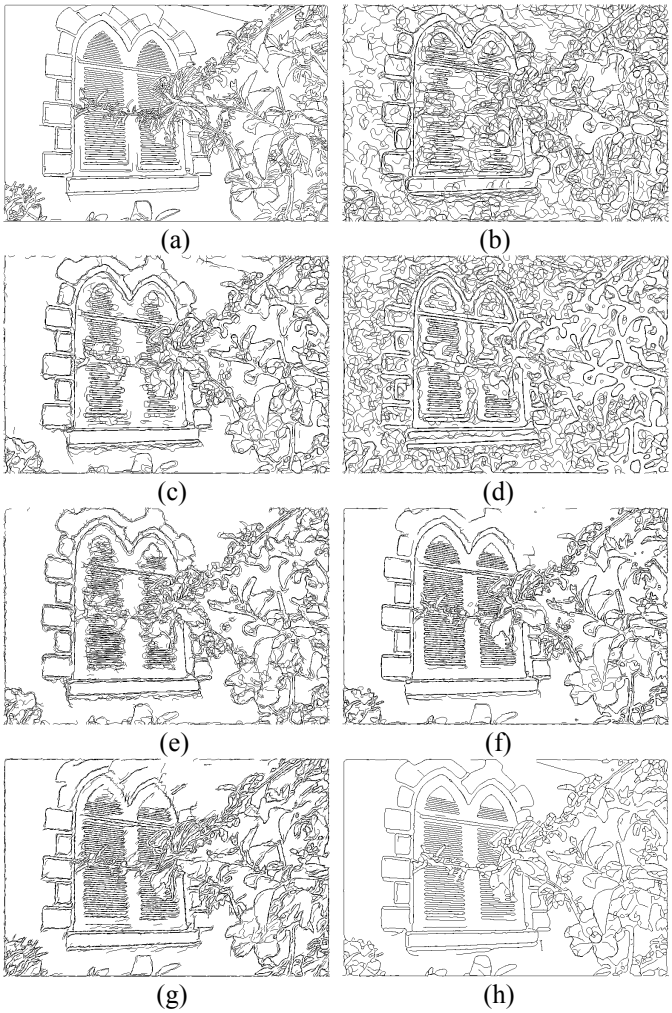

Fig. 15. Edges of degraded Flowers-Window image: (a) Original image; (b) Alvarez-Mazorra filter; (c) Kornprobst filter; (d) Gilboa filter ; (e) Fu filter; (f) Bettahar-Stambouli filter; (g) Tschumperlé-Deriche filter; (h) Proposed filter.

To characterize these results in a more precise way, we have focused our attention on a part of the border of the glasses as seen in fig. 17 where there are two main regions, the glass and the face. Then, we have computed three numerical indicators:

- the number of regions.
- the average size of the small regions. By small regions, we mean regions that are not the two main regions, i.e. the face and the glass.
- the sum of the color distance (denoted D_{color}) of these small regions to the two main regions, defined by:

$$D_{Color} = \sum_{k} \min(dist(C_{R1}, C_{Rk}), dist(C_{R2}, C_{Rk})) \times |R_k|$$

where C_{R1} and C_{R2} denote the color of the two main regions R_1 and R_2, C_{Rk} is the color of a small region R_k, k is the small region index , *dist(.)* is the Euclidean distance in the RGB space and $|R_k|$ is the size of the region R_k.

The last indicator is a measure of the false color importance. Indeed, if a small region has a color which is far from the color of R_1 and R_2, it will have a large contribution to D_{color}. Table 1 presents the results.

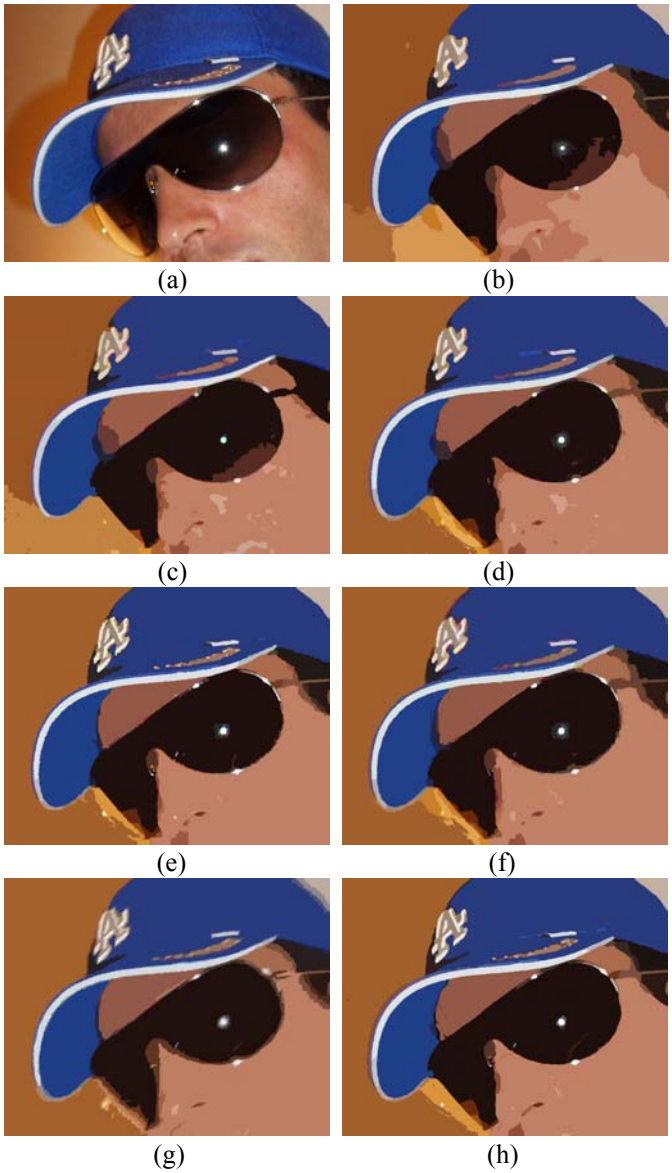

Fig. 16. Segmentation of Face image: (a) Non noisy initial image; (b) Alvarez-Mazorra filter 2442 regions; (c) Kornprobst filter 2385 regions; (d) Gilboa filter 2198 regions; (e) Fu filter 2071 regions; (f) Bettahar-Stambouli filter 2198 regions; (g) Tschumperlé-Deriche filter 1434 regions; (h) Proposed filter 2959 regions.

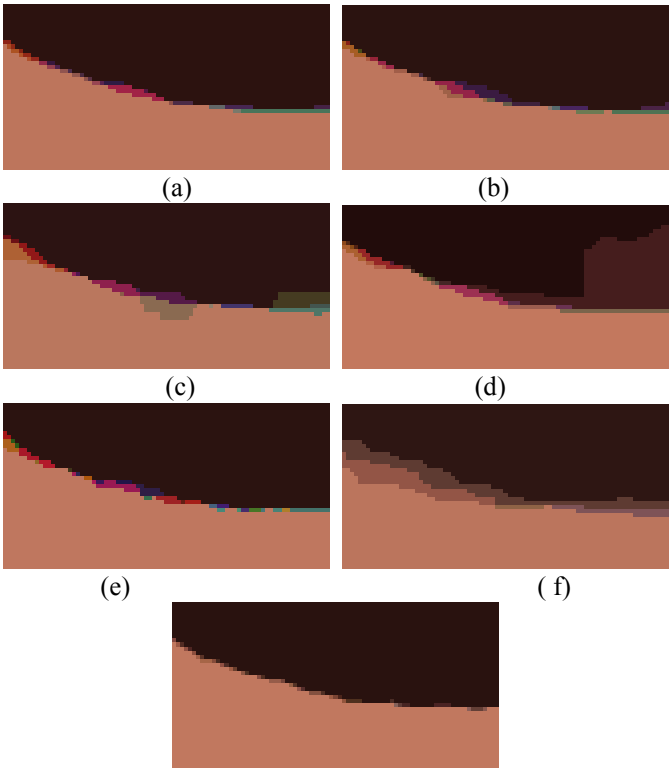

Fig. 17. Enlargement of Segmentation of Face image: (a) Alvarez-Mazorra filter; (b) Kornprobst filter; (c) Gilboa filter; (d) Fu filter; (e) Bettahar-Stambouli filter; (f) Tschumperlé-Deriche; (g) Proposed filter.

Method	Region number	Average size of small regions	D_{color} ($x10^{-3}$)
Alvarez-Mazorra	22	3	8.9
Kornprobst	57	5	9.58
Gilboa	26	23	27.8
Fu	54	12	15.8
Bettahar-Stambouli	68	4	10.9
Tschumperlé-Deriche	6	5	25.0
Proposed method	42	1	3.3

Table 1. Comparison of region segmentation performance on a small area of Face image.

Considering the proposed method, it can be seen that, despite the number of regions being large, these non wanted regions are small (average size is only one pixel) and their colors are close to the color of one of the two main regions (D_{color} is three times lower than the smaller value provided by other approaches).

By considering Flowers-Window image with 500 iterations (fig. 11), table 2 gives the execution time of all studied filters using a video machine Intel Core I7 4, 3GHz 24GO RAM Ubuntu 64 bit with matlab code. As no optimization has been done in our codes, the results are to be considered in a relative way.

Method	Execution time
Alvarez-Mazorra	2'14"
Kornprobst	3'56"
Gilboa	4'11"
Fu	5.23"
Bettahar-Stambouli	7'18"
Tschumperlé-Deriche	27'00"
Proposed	6'43"

Table 2. Comparison of the time execution of Flowers-Window image.

In this table, first it can be noted a wide diversity between the execution times of the different marginal approaches, Alvarez-Mazorra filter being the fastest and Bettahar-Stambouli filter the slowest. Secondly, it interesting to note that our vector approach is a little bit faster than the Bettahar-Stambouli marginal approach. It means that avoiding false colors does not increase the computation time. On the contrary, Tschumperlé-Deriche approach, which is also a vector approach, is the slowest approach

V. Conclusion

We have proposed a novel filter of coupling shock filter to curvature diffusion for color image enhancement in RGB space, which is based on using single vectors for all components of the image. This filter produces a selective smoothing reducing efficiently noise and sharpens edges. Our analysis shows that the proposed method is more efficient than Alvarez-Mazorra, Kornprobst, Gilboa, Fu, Bettahar-Stambouli and Tschumperlé-Deriche models at color image restoration in presence of blur and noise simultaneously. In that it denoises homogeneous parts of the multi-valued image, while it keeps edges enhanced. However, due to the fact of using single vectors with the specific reaction, our filter doesn't create false colors that can appear when each component of the image is enhanced separately.

Appendix: Numerical Implementation

We use finite difference to compute the different derivatives. Thus for p=1,2,3, the discrete image u_p can be regarded as a vector $[1\times MN]$, whose components u_{pi}, $i\in[1, \ldots, MN]$ display the grey values at the pixels. Pixel i represents the location x_i. Let h denote the discretization grid size. We employ discrete times $t_k=\tau k$, where k is a positive integer and τ is the time step size. By $u_{p_i}^k$, $v_{p_i}^k$, $\left|\nabla u_p\right|_i^k$, $\left|\nabla u\right|_i^k$, g_i^k, $\left|\nabla f\right|_i^k$, $\left(u_{p_{\eta\eta}}^k\right)_i$, $\left(u_{p_{\xi\xi}}^k\right)_i$, $\left(u_{\eta\eta}^k\right)_i$, $\left(u_{\xi\xi}^k\right)_i$ and $sign_i^k$ denote approximations of $u_p(x_i,t_k)$, $v_p(x_i,t_k)$, $|\nabla u_p|$, $|\nabla u|$, $g(|\nabla u_\sigma|)$, $\left|\nabla f(|\nabla u_\sigma|)\right|$, $u_{p_{\eta\eta}}$, $u_{p_{\xi\xi}}$, $u_{\eta\eta}$ $u_{\xi\xi}$ and $sign(G_\sigma * u_{\eta\eta})$ respectively.

For the implementation of temporal derivatives respecting to the component p, we use:

$$\frac{\partial u_p}{\partial t}=\frac{u_p^{k+1}-u_p^{k}}{\tau},\ \frac{\partial v_p}{\partial t}=\frac{v_p^{k+1}-v_p^{k}}{\tau} \tag{22}$$

In the first step, we compute the second equation:

$$\frac{v_{p_i}^{k+1}-v_{p_i}^{k}}{\tau}=-sign_i^k\left|\nabla u_p\right|_i^k \tag{23}$$

As mentioned above, v_p is the last value of u_p. So, we can write:

$$\frac{v_{p_i}^{k+1}-u_{p_i}^{k}}{\tau}=-sign_i^k\left|\nabla u_p\right|_i^k \tag{24}$$

Now, we are able to determine $v_{p_i}^{k+1}$, hence:

$$v_{p_i}^{k+1}=u_{p_i}^{k}-\tau\, sign_i^k\left|\nabla u_p\right|_i^k \tag{25}$$

At each iteration, we have a value of $v_{p_i}^{k+1}$, that will be injected in the first equation within the proposed model.

For the implementation of $|\nabla u_p|$ in the shock equation, we use minmod function *m(a,b)*:

$$m(a,b)=\begin{cases} sign(a)\min(|a|,|b|) & \text{if } ab>0 \\ 0 & \text{otherwise} \end{cases} \tag{26}$$

and

$$\left|\nabla u_p\right|_i^k=\frac{1}{h}\sqrt{\left(m\left(\delta_+^x u_{p_i}^k,\delta_-^x u_{p_i}^k\right)\right)^2+\left(m\left(\delta_+^y u_{p_i}^k,\delta_-^y u_{p_i}^k\right)\right)^2} \tag{27}$$

where δ_-^x and δ_+^x (δ_-^y and δ_+^y) are backward and forward differences of $u_{p_i}^k$ in x direction (y direction).

However, for $u_{p_{\eta\eta}}$ and $u_{p_{\xi\xi}}$, we use central differences to discretize all derivatives such as :

$$u_{p_{\eta\eta}}=\frac{u_{p_{xx}}^k\left(u_{p_x}^k\right)^2+2\,u_{p_{xy}}^k u_{p_x}^k u_{p_y}^k+u_{p_{yy}}^k\left(u_{p_y}^k\right)^2}{\left(u_{p_x}^k\right)^2+\left(u_{p_y}^k\right)^2} \tag{28}$$

$$u_{p_{\xi\xi}}=\frac{u_{p_{xx}}^k\left(u_{p_y}^k\right)^2-2\,u_{p_{xy}}^k u_{p_x}^k u_{p_y}^k+u_{p_{yy}}^k\left(u_{p_x}^k\right)^2}{\left(u_{p_x}^k\right)^2+\left(u_{p_y}^k\right)^2} \tag{29}$$

In the other hand, we use a semi-implicit scheme with harmonic averaging to approximate the quasi-divergence term [34]:

$$|\nabla u|\,div\left(g\left(|\nabla u_\sigma|\right)\frac{\nabla u_p}{|\nabla u_\sigma|}\right)=|\nabla u|_i^k\sum_{j\in w(i)}\frac{2}{\left(\frac{|\nabla u|}{g}\right)_j^k+\left(\frac{|\nabla u|}{g}\right)_i^k}\,\frac{\left(u_{p_j}^k-u_{p_i}^k\right)}{h^2} \tag{30}$$

w(i) consists on the four neighbors of pixel *i* and

$$|\nabla u|=\sqrt{\sum_{l\in\{x,y\}}\sum_{p=1}^{3}\left(\left|\nabla u_{p_l}\right|_i^k\right)^2} \tag{31}$$

For the discretization of $|\nabla f|_i^k$, we use the following approximation:

$$|\nabla f|_i^k=\sqrt{\left(f_N^k-f_S^k\right)^2+\left(f_W^k-f_E^k\right)^2}\Big/2 \tag{32}$$

where f_N^k, f_S^k, f_W^k and f_E^k denote respectively north, south, west and east values of the function *f* in the neighbors of pixel *i*.

Therefore, the numerical implementation of the proposed model with reflecting boundary conditions will be given by:

$$\begin{cases} \dfrac{u_{p_i}^{k+1}-u_{p_i}^{k}}{\tau}=|\nabla u|_i^k\displaystyle\sum_{j\in w(i)}\frac{2}{\left(\frac{|\nabla u|}{g}\right)_j^k+\left(\frac{|\nabla u|}{g}\right)_i^k}\,\frac{\left(u_{p_j}^{k+1}-u_{p_i}^{k+1}\right)}{h^2}-\alpha\frac{\left(|\nabla f|_i^k\right)^2}{1+\left(|\nabla f|_i^k\right)^2\left(u_{\xi\xi}^k\right)_i^2}\left(u_{p_i}^{k+1}-v_i^{k+1}\right) \\ \dfrac{v_{p_i}^{k+1}-v_{p_i}^{k}}{\tau}=-sign_i^k\left|\nabla u_p\right|_i^k \end{cases} \tag{33}$$

thus

$$\begin{aligned} \frac{u_{p_i}^{k+1}-u_{p_i}^{k}}{\tau}=&|\nabla u|_i^k\sum_{j\in w(i)}\frac{2}{\left(\frac{|\nabla u|}{g}\right)_j^k+\left(\frac{|\nabla u|}{g}\right)_i^k}\,\frac{\left(u_{p_j}^{k+1}-u_{p_i}^{k+1}\right)}{h^2} \\ &-\alpha\frac{\left(|\nabla f|_i^k\right)^2}{1+\left(|\nabla f|_i^k\right)^2\left(u_{\xi\xi}^k\right)_i^2}\left(u_{p_i}^{k+1}-u_{p_i}^{k}+\tau\, sign_i^k\left|\nabla u_p\right|_i^k\right) \end{aligned} \tag{34}$$

because as mentioned above, $v_{p_i}^k=u_{p_i}^k$. From where (35):

$$\begin{aligned} u_{p_i}^{k+1}=&\tau\frac{|\nabla u|_i^k}{h^2}\sum_{j\in w(i)}\frac{2}{\left(\frac{|\nabla u|}{g}\right)_j^k+\left(\frac{|\nabla u|}{g}\right)_i^k}\,u_{p_j}^{k+1} \\ &-\tau\left(\frac{|\nabla u|_i^k}{h^2}\sum_{j\in w(i)}\frac{2}{\left(\frac{|\nabla u|}{g}\right)_j^k+\left(\frac{|\nabla u|}{g}\right)_i^k}+\alpha\frac{\left(|\nabla f|_i^k\right)^2}{1+\left(|\nabla f|_i^k\right)^2\left(u_{\xi\xi}^k\right)_i^2}\right)u_{p_i}^{k+1} \\ &+\left(1+\tau\alpha\frac{\left(|\nabla f|_i^k\right)^2}{1+\left(|\nabla f|_i^k\right)^2\left(u_{\xi\xi}^k\right)_i^2}\right)u_{p_i}^{k}-\tau^2\alpha\frac{\left(|\nabla f|_i^k\right)^2}{1+\left(|\nabla f|_i^k\right)^2\left(u_{\xi\xi}^k\right)_i^2}sign_i^k\left|\nabla u_p\right|_i^k \end{aligned}$$

Using matrix-vector notation [12,13,36], where $u_{p_i}^k$ and $|\nabla u_p|^k$ are considered as vectors [1x*MN*], we obtain at time $k\tau$:

$$u_p^{k+1}=\tau A\left(u^k\right)u_p^{k+1}+\left(I+\tau\alpha F\left(u^k\right)\right)u_p^k-\tau^2\alpha F\left(u^k\right)S\left(u^k\right)\left|\nabla u_p\right|^k \tag{36}$$

Hence by decomposing the matrix *A* in *x* and *y* directions, we obtain:

$$\left(I-\tau\sum_{l\in\{x,y\}}A_l\left(u^k\right)\right)u_p^{k+1}=\left[\left(I+\tau\alpha F\left(u^k\right)\right)u_p^k-\tau^2\alpha F\left(u^k\right)S\left(u^k\right)\left|\nabla u_p\right|^k\right] \tag{37}$$

where *I* denotes the unit matrix. Components of the matrix *F*, *S* and A_l are given by:

$$\hat{f}_{ij}\left(u^k\right)=\begin{cases} \dfrac{\left(|\nabla f|_i^k\right)^2}{1+\left(|\nabla f|_i^k\right)^2\left(u_{\xi\xi}^k\right)_i^2} & i=j \\ 0 & \text{otherwise} \end{cases} \tag{38}$$

$$\hat{s}_{ij}\left(u^k\right)=\begin{cases} sign\ {}_i^k & i=j \\ 0 & \text{otherwise} \end{cases} \tag{39}$$

$$\hat{a}_{ij}\left(u^k\right)=\begin{cases} \dfrac{|\nabla u|_i^k}{h^2}\dfrac{2}{\left(\dfrac{|\nabla u|}{g}\right)_j^k+\left(\dfrac{|\nabla u|}{g}\right)_i^k} & j\neq i,\ j\in w_l(i) \\ -\dfrac{|\nabla u|_i^k}{h^2}\displaystyle\sum_{m\in w_l(i)}\dfrac{2}{\left(\dfrac{|\nabla u|}{g}\right)_m^k+\left(\dfrac{|\nabla u|}{g}\right)_i^k}-\alpha\dfrac{\left(|\nabla f|_i^k\right)^2}{1+\left(|\nabla f|_i^k\right)^2\left(u_{\xi\xi}^k\right)_i^2} & j=i \\ 0 & \text{otherwise} \end{cases} \tag{40}$$

$w_l(i)$ represents the two neighboring pixels with respect to the direction $l\in\{x,y\}$. Boundary pixels may have only one neighbor.

However, the solution u_p^{k+1} cannot be directly determined from the scheme (37). Instead, it requires solving a linear system of equations. Its solution is formally given by:

$$u_p^{k+1}=\left(I-\tau\sum_{l\in\{x,y\}}A_l\left(u^k\right)\right)^{-1}\left[\left(I+\tau\alpha F\left(u^k\right)\right)u_p^k-\tau^2\,\alpha F\left(u^k\right)S\left(u^k\right)\left|\nabla u_p\right|^k\right] \tag{41}$$

We can remark that the matrix $B=\left(I-\tau\sum_{l\in\{x,y\}}A_l\left(u^k\right)\right)$ is strictly diagonally dominant:

$$\left|b_{ii}\right|\succ\sum_{j\neq i}\left|b_{ij}\right| \tag{42}$$

therefore, it is invertible [37,38].

REFERENCES

[1] A. Rosenfeld and A. C. Kak, *Digital Picture Processing*, Academic Press, San Diego, CA, 1976.

[2] R. C. Gonzalez and P. Wintz, *Digital Image Processing*, Addison-Wesley, Reading, MA, 1977.

[3] S. Geman and D. Geman, "Stochastic relaxation, Gibbs distributions and the Bayesian restoration of images", *IEEE Trans. Pattern Anal. Mach. Intell.*, vol. 6, no. 6, pp. 721-741, 1984.

[4] H. Kaiqi, W. Zhenyang, W. Qiao, "Image enhancement based on the statistics of visual representation", *Image Vision Comput.*, vol. 23, no. 1, pp. 51–57, 2005.

[5] K. Dabov, A. Foi, V. Katkovnik and K. Egiazarian, "Image denoising by sparse 3D transform-domain collaborative filtering", *IEEE Trans. Image Process*, vol. 16, no. 8, pp. 2080-2095 , 2007.

[6] G. Y. Chen and T. D. Bui, "Multi-wavelet de-noising using neighboring coefficients", *IEEE Signal Process. Lett.* , vol.10, no.7, pp. 211-214, 2003.

[7] V. Strela, P. N. Heller, G. Strang, P. Topiwala and C. Heil, "The application of multiwavelet filter banks to image processing", *IEEE Trans. Image Process.*, vol. 8, no. 4, pp. 548–563, 1999.

[8] P. Perona and J. Malik, "Scale-space and edge detection using anisotropic diffusion", *IEEE Trans. Pattern Anal. Mach. Intell.,* vol. 12, no. 7, pp. 629-639, 1990.

[9] L. Alvarez, P. L. Lions, M. Morel and T. Coll, "Image selective smoothing and edge detection by nonlinear diffusion II*", SIAM J. Numer. Anal.*, vol. 29, no. 3, pp. 845-866, 1992.

[10] G. Aubert and L. Vese, "A variational method in image recovery", *SIAM J. Numer. Anal.*, no. 34, vol. 5, 1948-1979, 1997.

[11] L. Rudin, S. Osher and E. Fatemi, "Nonlinear total variation based noise removal algorithms", *Physica D*, vol. 60, no. 1-4, 259-268, 1992.

[12] F. Catté, P. L. Lions, M. Morel and T. Coll, "Image selective smoothing and edge detection by nonlinear diffusion", *SIAM J. Numer. Anal.*, vol. 29, no. 1, pp. 182-193, 1992.

[13] J. Weickert, B. M. ter Haar Romeny and M. A. Viergever, "Efficient and reliable schemes for nonlinear diffusion filtering", *IEEE Trans. Image Process.*, vol. 7, no. 3, pp. 398-410, 1998.

[14] R. Whitaker and X. Xue, "Variable-conductance level-set curvature for image denoising", in Proc. the International Conference on Image Processing, Thessaloniki, 2001, vol. 3, pp. 142-145.

[15] D.Tschumperlé, "Fast Anisotropic Smoothing of Multi-Valued Images using Curvature-Preserving PDE's", *Int. J. Comput. Vision*, vol. 68, no. 1, pp. 65--82, 2006.

[16] S. Osher and L. I. Rudin, "Feature-oriented image enhancement using shock filters", *SIAM J. Numer. Anal.*, vol. 27, no. 4, pp. 919-940, 1990.

[17] L. Remaki and M. Cheriet, "Enhanced and restored signals as a generalized solution for shock filter models. Part I-existence and uniqueness result of the Cauchy problem", *J. Math. Anal. Appl.*, vol. 279, no. 1, 189-209, 2003.

[18] M. Cheriet and L. Remaki, "Enhanced and restored signals as a generalized solution for shock filter models. Part II-numerical study", *J. Math. Anal. Appl.*, vol. 279, no. 2, pp. 398-417, 2003.

[19] B. M. ter Haar Romeny, *Front-end vision and multi-scale image analysis*, Kluwer Academic Publishers, Berlin, 2003.

[20] L. Alvarez and L. Mazorra, "Signal and image restoration using shock filters and anisotropic diffusion", *SIAM J. Numer. Anal.*, vol. 31, no. 2, pp. 590-605, 1994.

[21] P. Kornprobst, R. Deriche and G. Aubert, "Image coupling, restoration and enhancement via PDE's", *in Proc. the International Conference on Image Processing,* Santa Barbara, 1997, vol. 2, pp. 458-461.

[22] G. Gilboa, N .Sochen and Y.Y .Zeevi, "Image enhancement and denoising by complex diffusion processes", *IEEE Trans. Pattern Anal. Mach. Intell.*, vol. 26, no. 8, pp. 1020-1036, 2004.

[23] S. Fu, Q. Ruan, W. Wang and J. Chen, "Region-based Shock-diffusion Equation for Adaptive Image Enhancement", *Lect. Notes Comput. Sc.*, vol. 4153, pp. 387-395, 2006.

[24] S. Bettahar and A.B. Stambouli, "Shock filter coupled to curvature diffusion for image denoising and sharpening", *Image Vision Comput.*, vol. 26, no.11, pp. 1481-1489, 2008.

[25] A. Trémeau, C. Fernandez-Maloigne and P. Bonton, *Image numérique couleur de l'acquisition au traitement*, Duno, Paris, 2004.

[26] S. Di Zenzo, "A note on the gradient of multi-images", *Comput. Vision Graph.*, vol. 33, no. 1, pp. 116–125, 1986.

[27] H. C. Lee and D. R. Cok, "Detecting Boundaries in a Vector Field", *IEEE Trans. Signal Process.*, vol. 39, no. 5, pp. 1181-1194, 1991.

[28] G. Sapiro and D. Ringach, "Anisotropic diffusion of multivalued images with applications to color filtering", *IEEE Trans. Image Process.*, vol. 5, no. 11, pp. 1582–1586, 1996.

[29] B. Tang, G. Sapiro and V. Caselles, "Color image enhancement via chromaticity diffusion", *IEEE Trans. Image Process.*, vol. 10, no. 5, pp. 701-707, 2001.

[30] D. Tschumperlé and R. Deriche, "Diffusion PDE's on Vector-valued images: Local approach and geometric viewpoint", *IEEE Signal Process. Mag.*, vol. 19, no. 5, pp. 16-25, 2002.

[31] J. Weickert, "Coherence-enhancing shock filters", Lect*. Notes Comput. Sc.*, vol. 2781, pp. 1-8, 2003.

[32] J. Weickert, "Coherence-enhancing diffusion of colour images", *Image Vision Comput.*, vol. 17, no. 3-4, pp. 199-210, 1999.

[33] Y. Hou, C. Zhao, D. Yang and Y. Cheng, "Comment on Image Denoising by Sparse 3D Transform-Domain Collaborative Filtering", *IEEE Trans. Image Process*, vol. 20, no. 1, pp 268-270, 2011.

[34] Z. Wang, A. C. Bovik, H. R. Sheikh and E. P. Simoncelli, "Image Quality Assessment: From Error Visibility to Structural Similarity", *IEEE Trans. Image Process.*, vol. 13, no. 4, pp. 600-612, 2004.

[35] D. H. Ballard and C. M. Ballard, *Computer Vision*, Prentice Hall, 1982.

[36] J. Weickert, "Application of nonlinear diffusion in image processing and computer vision", Acta Mathematica Universitatis Comenianae, vol. 70, no. 1, pp. 33-50, 2001.

[37] P. G. Ciarlet, *Introduction à l'analyse numérique matricielle et à l'optimisation*, Dunod, Paris, 1998.

[38] D. Euvrard, *Résolution numérique des équations aux dérivées partielles*, 3ème Edition, Masson, Paris, 1994.

Salim Bettahar received the engineer degree in electronics in 1998, and the degree of Magister and PhD in 2002 and 2009 respectively in non destructive testing and imagery. He is currently an assistant professor at the University of Sciences and Technology of Oran, Algeria. His research interest concerns the application of partial differential equations in image processing and computer vision. He is a member of the electrical engineering laboratory of Oran, Algeria.

Amine Boudghene Stambouli is a graduate of the University of Sciences and Technology of Oran, Algeria in 1983. He received his master's degree in modern electronics in 1985 and his PhD in optoelectronics in1989 at the University of Nottingham, England. He is a full Professor at the University of Sciences and Technology of Oran. His research interests include at present the images processing related to renewable energies and their environment impacts. He is a member of the electrical engineering laboratory of Oran, Algeria.

Patrick Lambert received the engineer degree in electrical engineering in 1978, and the PhD degree in signal processing in 1983, both from the National Polytechnic Institute of Grenoble, France. He is currently a Full Professor at the School of Engineering of University of Savoie, Annecy, France and a member of the Informatics, Systems, Information and Knowledge Processing Laboratory (LISTIC), Annecy, France. His research interests include color image processing and video analysis.

Alexandre Benoit received the engineer degree in informatics and electronics in 2003 and the PhD degree in image and signal processing in 2007. He is currently an assistant professor at the University of Savoie, Annecy, France. He teaches informatics and is member of the Informatics, Systems, Information and Knowledge Processing Laboratory (LISTIC). His research interest concerns image processing and information fusion for high semantic level visual scene interpretation.